A bispecific nanobody for the treatment of von Willebrand disease type 1

Ivan Peyron, Caterina Casari, Geneviève Mccluskey, Stéphanie Roullet, Vincent Licari, Emilie Bocquet, Claire Auditeau, Mélanie Y Daniel, Sophie Susen, Olivier D Christophe, et al.

A bispecific nanobody for the treatment of Von Willebrand disease-type 1

Ivan Peyron[1], Caterina Casari[1], Geneviève McCluskey[1], Stephanie Roullet[1,2], Vincent Licari[1], Emilie Bocquet[1], Claire Auditeau[1,3], Mélanie Y Daniel[4], Sophie Susen[4,5], Olivier D Christophe[1], Peter J Lenting[1], Cécile V Denis[1,6]

[1]Université Paris-Saclay, INSERM, Hémostase Inflammation Thrombose HITh U1176, 94276, Le Kremlin-Bicêtre, France

[2]Département d'Anesthésie Réanimation, Hôpital Paul Brousse, Assistance Publique-Hôpiteaux de Paris, Université Paris-Saclay, Villejuif, France

[3]Service d'Hématologie Biologique, Hôpital Necker Enfants Malades AP-HP, Paris, France

[4]Hematology and Transfusion Department, INSERM U1011, Centre Hospitalier Universitaire de Lille, Institut Pasteur de Lille, Université de Lille, European Genomic Institute for Diabetes, Lille, France

[5]French Reference Center for von Willebrand disease (CRMW), Lille, France

[6]Centre Hospitalier Régional Universitaire de Nancy, 54000 Nancy, France

Running title: KB-V13A12 increases VWF plasma levels

Corresponding author:
Peter J. Lenting, PhD
Inserm U1176
80 rue du Général Leclerc
94276 Le Kremlin-Bicetre
France
Tel: +331 49 59 56 00
E-mail: peter.lenting@inserm.fr

Abstract: 240 words

Main text: 3980 words

Figures: 7

References: 45

Data sharing: Data are available upon reasonable request to the corresponding author

Key points

- VWD-type 1 may be associated with clinically significant bleeding symptoms and reduced quality-of-life, while prophylactic treatment is rare
- Subcutaneous injection of nanobody KB-V13A12 increases endogenous VWF levels 2-fold for 10 days and restores hemostasis in VWD-type 1 mice

Abstract

Von Willebrand disease (VWD)-type 1 is a bleeding disorder characterized by a quantitative deficiency of functional von Willebrand factor (VWF). We designed a novel bispecific nanobody, named KB-V13A12, that aims to increase endogenous VWF levels by bridging it to albumin. KB-V13A12 comprises two single-domain antibodies, one targeting VWF and one targeting albumin. VWF bound efficiently to the albumin/KB-V13A12 complex (2.0±0.4 nM) in immunosorbent assays and binding was stable at pH 5.6 and 7.4. VWF ristocetin activity and factor VIII binding remained unaffected in the presence of a 100 to 200-fold molar excess of KB-V13A12/albumin. Humanized VWD-type 1 mice were used for in vivo analysis. A single subcutaneous dose of KB-V13A12 (5 mg/kg) was associated with a nanobody half-life of 3.0±0.7 days and dose-dependently increased VWF in VWD-type 1 mice 1.4 to 2.1-fold for up to 14 days. FVIII activity was also increased during this period. The VWF-propeptide/VWF-antigen ratio (a marker for VWF clearance) was significantly reduced in the presence of KB-V13A12, suggesting that delayed clearance contributes to increased VWF levels. Clearance experiments in wild-type mice using recombinant VWF pre-incubated with KB-V13A12 indeed confirmed a prolonged survival, while this prolongation was absent in FcRn-deficient-mice. Finally, treatment with KB-V13A12 resulted in a significantly improved bleeding tendency in VWD-type 1 mice when using the saphenous vein puncture-model. In conclusion, KB-V13A12 is a bispecific nanobody that efficiently increases functional levels of endogenous VWF, and could be a therapeutic option to treat VWD-type 1.

Introduction

Von Willebrand disease (VWD)-type 1 is an inherited bleeding disorder characterized by a partial quantitative deficiency of von Willebrand factor (VWF), with VWF platelet-dependent activity and VWF antigen (VWF:Ag) being proportionally decreased.[1,2] A genetic epidemiological population-based study initially projected the worldwide prevalence of VWD-type 1 at 74 per 1,000 people.[3] However, a recent extension of the study, which included over 800,000 individuals, revealed that 11 per 1,000 (1.1%) are likely to exhibit clinically and laboratory-defined VWD due to variable expression.[4]

The bleeding tendency in VWD-type 1 patients is reputedly less severe compared to VWD-type 2 and VWD-type 3 patients.[2] However, despite this milder hemorrhagic diathesis, bleeding is not uncommon in these patients, with epistaxis being reported in 39-53% and post-dental extraction bleeding in 42-53% of VWD-type 1 patients.[5] Menorrhagia affects about 80% of VWD-type 1 patients who experience menstruation, and an increased Bleeding Assessment Tool-score was found in 94% of adolescent VWD-type 1 patients with heavy menstrual bleeding.[5,6] Importantly, the presence of clinically significant bleeding symptoms is not restricted to patients with severe forms of VWD-type 1, because large cohort studies have demonstrated that these also occur in patients with mildly reduced VWF levels (30-50% residual VWF).[7,8]

The majority of bleeds in VWD-type 1 patients are treated using desmopressin, an antidiuretic that induces VWF release from endothelial storage-organelles. It is indicated for nosebleeds, heavy menstrual bleeding, gingival bleeding or dental extractions and surgery.[2] Desmopressin use may result in mild to severe side effects, especially in elderly patients having cardiovascular comorbidities, which may lead to discontinuation of its use.[9] Transfusion with VWF concentrates is recommended when desmopressin therapy is not effective or contra-indicated.[2] Despite the availability of effective therapeutic options, prophylactic treatment is rare. Consequently, frequent minor bleeds greatly affect the quality of life of VWD-type 1 patients, which is illustrated by a significant impact on the mental and physical well-being of these patients.[10-14] There is thus a need for a novel therapeutic approach that allows for prophylactic treatment without the burden of frequent intravenous injections.

Given that VWF is fully functional in VWD-type 1 patients and is only restricted by its concentration, we hypothesized that increasing endogenous VWF levels by prolonging its half-life could be a potential option. Pharmacokinetic modulation is a common therapeutic strategy used previously to prolong the half-life of therapeutic agents. Indeed, several Fc- or albumin-fusions proteins have been developed, making use of the neonatal Fc-receptor (FcRn)-recycling pathway to achieve such half-life prolongation.[15] FcRn-recycling is initiated by pinocytosis of Fc- or albumin-fusion proteins.[16] Subsequent acidification of early endosomes promotes the binding of Fc or albumin to FcRn, preventing the release of these proteins into the lysosomal degradation pathway. Instead, FcRn-protein complexes are sorted into tubulovesicular transport vesicles, the majority of which are recycled back to the plasma membrane undergoing exocytosis. Exposure to physiological pH dissociates the proteins from FcRn, releasing them back into the circulation.[17]

By analogy to this mechanism, we designed an approach that would bridge endogenous VWF to circulating albumin, thus allowing the complex to be recycled via the FcRn-pathway. We previously reported initial data, showing that this molecule (KB-V13A12) is able to increase endogenous levels of

the VWF/FVIII complex, and that this increase reduces the bleeding tendency in humanized VWD-type 1 mice (hVWD1-mice).[18] Here we provide an extended analysis of KB-V13A12, showing its capacity to link VWF to albumin, and to delay VWF clearance in a FcRn-dependent manner. Furthermore, recycled VWF proved functional in *ex vivo* perfusion experiments and in an *in vivo* bleeding model.

Materials and methods

A detailed description of the materials and methods can be found in the online supplementary information.

Ethics statement

Animal housing and experiments were performed in accordance with French regulations and the experimental guidelines of the European Community. This project was approved by the local ethical committee of Université Paris-Saclay (Comité d'Ethique en Expérimentation Animale n°26, protocole APAFIS#32699-2021081611421076-v1).

Mice

C57B6/J VWF-deficient (VWF^{KO})-mice and 129S humanized VWD-type 1 (hVWD1)-mice have been described previously.[18,19] Wild-type (WT)-mice were on a C57B6/J or 129S background. C57B6/J FcRn-deficient ($FcRn^{KO}$)-mice were obtained from Charles River (Saint-Germain-Nuelles, France).

Proteins

Nanobodies KB-VWF-013, KB-OptiAlb12 and KB-V13A12 were expressed in *E-coli* WK6 bacteria and purified as described.[18] KB-OptiAlb12 and KB-V13A12 bind to human albumin (HSA) and murine albumin (MSA), but not to bovine albumin (BSA), and both contain a C-terminal His-tag and a cMyc-tag.

Clearance experiments

Clearance of biotinylated KB-VWF-006bv: Biotinylated nanobody KB-VWF-006bv (bt-KB-VWF-006bv) was infused (5 mg/kg) via an intravenous retro-orbital injection in VWF^{KO}-deficient mice or their wild-type littermates. Residual plasma levels of bt-KB-VWF-006bv were determined using streptavidin-coated microtiter wells. Bound nanobodies were probed using peroxidase-labeled polyclonal rabbit anti-haemagglutinin antibodies.

Clearance of KB-V13A12: KB-V13A12 (5 mg/kg) was infused via an intravenous retro-orbital injection in WT-mice or given subcutaneously to hVWD-1 mice. Residual plasma levels of KB-V13A12 were determined via quantitative western-blotting using biotinylated AffiniPure polyclonal goat anti-alpaca IgG-VHH antibodies and IRDye-680RD Streptavidin, subsequently. Membranes were imaged and analyzed using the Typhoon NIR laser-scanner platform and the ImageQuantTL v10.2 software (Cytiva, Velizy Villacoublay, France). The lower limit of detection of this assay was 0.1 μg/ml KB-V13A12 in the undiluted plasma sample, with the reference range being linear up to 50 μg/ml.

Clearance of recombinant VWF: Recombinant VWF (0.5 mg/kg) was given intravenously via retro-orbital injection in the presence of KB-V13A12 (5 mg/kg; representing an 82-fold molar excess over VWF) or a control nanobody (5 mg/kg) to C57B6 WT-mice or $FcRn^{KO}$-mice. Residual plasma levels of human VWF were determined using a human VWF-specific antigen assay.

In silico modeling

Molecular modeling of KB-VWF-013 and KB-OptiAlb12 was outsourced to MabSilico (www.mabsilico.com, Tours, France). A model of KB-V13A12 was generated combining the Modeller-software created nanobody structures using AlphaFold-2.[20] PyMOL-software (version 3.1.3.1) was used to align the structure of KB-V13A12 to those of albumin (PDB-deposit 1AO6)[21] and the VWF/FVIII complex (PDB: 7KWO)[22] as well as to those of albumin with the VWF/Glycoprotein Ibα complex (using PDB: 7ZWH and PDB: 1M10).[23]

Saphenous vein puncture model

The saphenous vein pinch model was conducted essentially as described.[18,24]

Parallel plate flow perfusion

Murine blood half-diluted in Tyrode's buffer was labeled with rhodamine 6G. Thrombus formation was evaluated after perfusion assay on a fibrillar collagen matrix under arterial shear conditions (shear rate of 3000 s^{-1}).[25]

Statistical analysis

All data are presented as mean±standard deviation (mean±SD) unless indicated otherwise. Number (*n*) refer to the number of independent experiments or animals. The statistical analysis was performed using Prism10 software for Mac (GraphPad, La Jolla, CA). One-way analysis of variance (1-way ANOVA) followed by Tukey's or Dunnett's multiple comparison test was performed when comparing multiple groups. Pairwise analysis was performed using the unpaired Student's t-test, with Welch-correction where appropriate.

Results

Design of bispecific nanobody KB-V13A12

To bridge VWF to albumin, we designed a bispecific nanobody, KB-V13A12. This bispecific nanobody comprises one nanobody targeting VWF and another targeting albumin. The VWF-targeting nanobody, KB-VWF-013, has been previous described, and binds to the D'D3-region.[26] The albumin-targeting nanobody, KB-OptiAlb12 is a llama-derived nanobody that cross-reacts with both human and murine albumin. KB-V13A12 displayed efficient binding to immobilized human recombinant VWF (half-maximal binding 0.8±0.1 nM; Figure 1A). In addition, KB-V13A12 bound to both human and murine albumin (half-maximal binding 2.4±0.3 nM and 14±2 nM, respectively, Figure 1B). To verify its ability to bridge VWF and albumin, immunosorbent assays were performed. Immobilized HSA or MSA (0.1 μM) were incubated with various concentrations of KB-V13A12 (0-50 nM) and subsequently with a fixed concentration of VWF (24 nM; Figure 1C). Alternatively, the KB-V13A12 concentration was kept constant (0.2 μM) and VWF concentrations were varied (0-36 nM; Figure 1D). In both approaches, efficient dose-dependent binding was observed. For Figure 1C, half-maximal binding was obtained at 0.9±0.1 nM and 6.2±0.3 nM for HSA and MSA, respectively. For Figure1D, half-maximal binding was obtained at 4.1±0.3 nM and 1.5±0.2 nM for HSA and MSA, respectively. Importantly, when using variable VWF concentrations, the response was similar, irrespective whether binding conditions were performed at pH=7.4 or pH=5.6 (Figure 1D). Thus, KB-V13A12 effectively bridges human VWF to human or murine albumin *in vitro*.

Modelling of the albumin/KB-V13A12/VWF-D'D3/FVIII complex

To visualize the interaction between KB-OptiAlb-12 and KB-VWF-013 with albumin and the VWF-D'D3 domain, respectively, molecular modeling was performed using existing structures of human albumin and the human VWF-D'D3/FVIII complex. 3D-models for KB-OptiAlb-12 and KB-VWF-013 were generated using PDB-deposits 7CJ2 and 4TVS as template, respectively. In silico docking-procedures pointed to a binding site of KB-OptiAlb-12 involving albumin residues Thr^{491}-Lys^{499}, Glu^{516}-Phe^{526} and His^{559}-Lys^{565}, which are located in domain III of albumin (Figure 2A). For KB-VWF-013, its epitope was found to include residues His^{1114}-Val^{1155} and His^{1176}-Pro^{1197} (Figure 2B). We then used AlphaFold-2 to generate a model of KB-V13A12. Subsequently, PyMOL-software was used to create models of KB-V13A12 with albumin and the VWF-D'D3/FVIII complex and of KB-V13A12 with albumin and the VWF-D3A1/GpIbα complex (Figure 2C-D). These models suggest that KB-V13A12 binds to the D3-domain, without sterically interfering with the interaction between VWF and FVIII or GpIbα.

KB-V13A12 leaves VWF function unaffected and binds to VWF D'D3 mutants

KB-VWF-013 was previously selected because of its non-inhibitory behavior[26], and AlphaFold-2 generated models suggest that KB-V13A12 indeed leaves FVIII and GpIbα binding unaffected. This was further validated in functional assays for ristocetin-induced GpIbα binding (VWF:GpIbR) and FVIII binding. When using the VWF:GpIbR assay, GpIbα binding remained unchanged upon titration of a large molar excess of KB-V13A12 (0-100 μg/ml, 0-3.3 μM) into human plasma (Figure 2E). Furthermore, binding of FVIII to immobilized VWF was unaffected in the presence of 1.7 μM KB-

V13A12, HSA or complexes thereof (Figure 2F). Given its epitope, we also investigated binding of KB-V13A12 to various VWF-D'D3 mutants. VWF present in plasma of patients with mutations in the D'D3-region was immobilized into microtiter-wells coated with anti-VWF antibodies and bound VWF was then probed with KB-V13A12. Out of the 8 mutants tested (p.C1130F, p.C1130W, p.C1173F, p.Y1146C, p.T1156M, p.C1196R, p.R1205H and p.R1205L), none displayed reduced binding of KB-V13A12 (Supplemental figure S1). Thus, KB-V13A12 is able to efficiently bind a variety of VWF D'D3 variants, while leaving FVIII binding and GpIbα binding unaffected.

In vivo survival of KB-V13A12

Bivalent or bispecific nanobodies have a molecular weight (30-35 kDa) that would force rapid renal clearance unless the nanobody is able to bind circulating ligands. For example, intravenous infusion of a bivalent VWF-binding nanobody (KB-VWF-006bv)[27] in VWF-deficient mice is associated with a half-life of <10 minutes (Figure 3A). In contrast, intravenous infusion of the same nanobody (which efficiently binds murine VWF) into wild-type mice results in a secondary half-life of 2.1 h, close to the half-life of VWF in mice (Fig. 3A).[28] When given to WT-mice intravenously, the albumin-binding nanobody KB-V13A12 displayed a secondary half-life of 36h, which is similar to the reported half-life of MSA (Fig. 3A).[29] We next explored the in vivo survival of KB-V13A12 following subcutaneous injection. A single dose (5 mg/kg) was given to VWD-type 1 mice, and its presence in plasma was monitored for 14 days. Already at 5 min after injection, KB-V13A12 could be detected in plasma, and KB-V13A12 remained present up to 14 days. Maximum levels of KB-V13A12 were found after 24 h at a concentration of 0.9±0.2 μM (Figure 3B). In terms of molar ratio of KB-V13A12 over VWF, a 154±28-fold molar excess was obtained 24 h after injection, and KB-V13A12 remained in excess over VWF until day 14 (molar ratio=2.6±1.1; Figure 3C). These data indicate that a single subcutaneous injection allows for a long-term presence of KB-V13A12 in the circulation, the majority of the time being in molar excess over VWF.

KB-V13A12 increases VWF and FVIII levels

Given the prolonged presence of KB-V13A12 in the circulation after a single subcutaneous dose, we then monitored if and how KB-V13A12 modulates VWF and concurrent FVIII levels in hVWD1-mice. Four different doses of KB-V13A12 (0.5, 2, 5 and 25 mg/kg) were administered subcutaneously to these mice and VWF and FVIII levels were monitored for 14 days. Apart from the lowest dose (0.5 mg/kg), all other doses were associated with a 2-fold increase of VWF (Figure 4A). Furthermore, the higher the dose, the longer VWF remained increased at these levels. At the two highest doses, VWF levels were still above starting levels at day 14 (5 mg/kg: 15.4±3.7 U/dl vs 11.3±1.8 U/dl; p=0.0026; n=12 and 25 mg/kg 19.1±4.3 U/dl vs 12.6. ±1.5 U/dl; p=0.0002; n=10). Increased VWF levels were associated with increased collagen binding, which returned to baseline at day 14 (Supplementary figure S2). Levels of FVIII, which circulates in complex with VWF, were also increased up to 1.5-fold in a dose-dependent manner (Figure 4B). Again, FVIII levels remained increased the longest when using higher doses of KB-V13A12.

KB-V13A12 reduces VWF clearance in an FcRn-dependent manner

We hypothesized that by bridging VWF to albumin, KB-V13A12 is able to prolong its circulatory half-life. It has previously been established that the changes in the ratio of the VWF propeptide (VWFpp) over VWF antigen is a marker for changes in VWF clearance.[30,31] We therefore compared ratios of VWFpp over VWF in hVWD1-mice before and three days after subcutaneous injection of KB-V13A12 (*ie.* when VWF has reached its maximum increase). The relative VWFpp/VWF ratio was markedly reduced at day 3 compared to before treatment (0.41±0.05 vs 1.0±0.20; n=4 p=0.0011; Figure 5A), suggesting that clearance of VWF is delayed in the presence of KB-V13A12. This was further assessed in clearance experiments using wild-type and FcRn-deficient mice in which recombinant VWF was pre-incubated with KB-V13A12 or a control nanobody before intravenous injection. In wild-type mice, the presence of KB-V13A12 resulted in a prolonged presence of recombinant VWF in the circulation compared to the use of the control nanobody (Area under the curve (AUC): 442±22 versus 153±33; n=3; p<0.0001; Figure 5B). In contrast, clearance of VWF in the presence of KB-V13A12 was no longer prolonged in the absence of FcRn (AUC=148±21; n=3; p=0.9952 vs VWF+control nanobody in wild-type-mice and p<0.0001 vs VWF+KB-V13A12 in wild-type mice), while clearance of VWF in the presence of the control nanobody in FcRn-deficient mice was unaffected (AUC=107±20; n=3; p=0.1853 vs wild-type-mice; Figure 5C-D).

KB-V13A12 improves in vitro thrombus formation

We next explored the capacity of KB-V13A12 to improve platelet adhesion in *ex vivo* perfusion experiments. First, blood from hVWD1-mice that were given 0.1 mg/kg rVWF (10 U/kg; giving a rise of 20 U/dl rVWF) or histamine (13 μmol/kg) was compared to blood of untreated hVWD1-mice. Treatment with rVWF or histamine resulted in a significant increase of platelet adhesion when blood was perfused over a collagen-coated surface. Surface coverage increased near 2-fold from 6.7±2.4% (n=8) to 11.3±1.7 % (n=4; p=0.039) and 11.2±3.5% (n=4; p=0.042; Figure 6A-B), respectively. When blood from hVWD1-mice treated with KB-V13A12 was analyzed, a similar 2-fold increased platelet adhesion was observed (13.0±3.5%; n=10; p=0.0003; Figure 6A-B). Together these data show that KB-V13A12 induces an increase of functional VWF, resulting in increased thrombus formation.

KB-V13A12 improves the hemostatic capacity of hVWD1-mice

We recently reported that treatment with KB-V13A12 reduces blood loss in hVWD1-mice in a tail clip-bleeding model.[18] Functionality of VWF was further explored in another bleeding model, *ie.* the saphenous vein puncture model. Two parameters were analyzed: the number of clots over a 30 min period and the maximal bleeding time during these 30 min. In terms of clots, hVWD1-mice produced significantly fewer clots than wild-type mice (8±5 (n=11) vs 19±7 (n=5); p=0.0289; Figure 7A). The maximal bleeding time was also significantly prolonged in hVWD1-mice: 11±7 min (n=11) vs 3±1 min (n=5; p=0.0007; Figure 7B). Upon treatment with KB-V13A12, both parameters were normalized to the level of wild-type mice: 17±7 clots (n=11; p=1.0 and p=0.0292 compared to wild-type and hVWD1-mice, respectively; Figure 7A) and 6±5 min (n=11; p=0.92 and p=0.0478 compared to wild-type and hVWD1-

mice, respectively; Figure 7B). These results further confirm that treatment with KB-V13A12 is associated with an improved hemostatic capacity of hVWD1-mice.

Discussion

Albumin and IgG are among the proteins with the longest circulatory half-life due to their interaction with FcRn, which prevents them from early endosomal degradation by recycling them back into the circulation. To take advantage of this mechanism, many therapeutic proteins have been fused to albumin or the FcRn-binding portion of IgG, *ie.* the Fc-domain. As such, these proteins generally display a markedly prolonged half-life. Here, we present a novel strategy in which we use a bispecific nanobody to capture an endogenous protein into the FcRn-recycling pathway by bridging this protein to circulating albumin. This will delay the clearance of the target protein, resulting in increased plasma levels. We believe that such strategy could be particularly useful for pathological conditions in which there is a partial quantitative deficiency of a plasma protein.

In this study we provide an example for VWD-type 1, a disease characterized by the presence of fully functional VWF at levels that are below the normal range. Linking VWF to albumin is not completely without precedent, given the brief description of a VWF-albumin fusion protein which showed a prolonged half-life compared to traditional VWF.[32] In our approach, we designed a bispecific nanobody with one arm targeting human VWF and a second arm targeting albumin. The albumin-binding nanobody (KB-OptiAlb12) is a humanized nanobody that efficiently recognizes human, primate and murine albumin. The advantage is therefore that same nanobody can be used in preliminary testing using mouse models as well in more advanced preclinical studies using primates and eventually in clinical evaluation using human patients. For the VWF-binding part, we used the previously described nanobody KB-VWF-013.[26] This nanobody is directed against the D'D3-region of VWF and is non-inhibitory of nature: it leaves VWF functions such as FVIII and Glycoprotein Ibα binding unaffected.

Combined into the bispecific nanobody KB-V13A12, this moiety efficiently bridges VWF to albumin. Albumin circulates at high concentrations in plasma (600 μM), and in the context of the high affinity of KB-OptiAlb12 for albumin (<5 nM), it is expected that >99% of the nanobody will circulate in complex with albumin, while the vast majority of albumin remains nanobody-free. Thus, variations in albumin concentrations will have little if any consequence on complex formation with the nanobody. Moreover, given that KB-VWF-013 binds human VWF also with high affinity (<5 nM), it seems conceivable that concentrations of KB-V13A12 exceeding 50 nM would result in >90% of VWF being incorporated in the ternary VWF/KB-V13A12/albumin complex, even when VWF concentrations are below the normal range.

High affinity binding to albumin is crucial to achieve a prolonged half-life. Vanderschuren *et al.* showed that there exists a strong correlation between the affinity of a ligand for albumin and the half-life extension for this ligand.[33] Moreover, a K_D value of 2 μM proved sufficient to achieve a half-life similar to that of albumin.[33] Given that the affinity of KB-V13A12 for MSA is in the nM-range, it is not surprising that this nanobody displays a circulatory half-life similar to that of MSA in mice, which is estimated to be between 29-35 h.[29,34] It remains to be investigated whether the half-life extension for VWF bound to the KB-V13A12/albumin complex will be as long.

We did not explore yet whether binding of the bispecific nanobody modulates the regular clearance pathways of VWF, as it will be part of a separate study. However, VWF contains multiple binding sites for numerous clearance-receptors, and it is possible that at least some of these receptors can still

interact with VWF that is complexed to KB-V13A12/albumin.[35-37] Akin to FcRn, however, these clearance receptors are predominantly expressed on macrophages and endothelial cells.[35-39] It cannot be excluded that after entering the clearance pathway and being released from the clearance-receptor upon acidification in the early endosomes, the VWF/KB-V13A12/albumin complex can actually start binding to FcRn, provided that the clearance-receptor and FcRn are present in the same early endosome. To do so, it is of course an absolute requirement that the VWF/KB-V13A12/albumin complex resists low pH-induced dissociation. When tested *in vitro*, we observed similar formation of this complex, irrespective whether binding was assessed at pH=5.6 or pH=7.4, suggesting that VWF remains partner of the VWF/KB-V13A12/albumin complex under both acidic and neutral conditions.

The notion that the VWF/KB-V13A12/albumin complex resists dissociation under acidic conditions is in agreement with the observation that increased VWF levels upon treatment with KB-V13A12 seem to be the result of a delayed clearance via FcRn-mediated recycling. Several experimental observations indeed point to delayed VWF clearance as the mechanism underlying increased VWF levels. First, VWF and its propeptide (VWFpp) circulate separately with a defined VWFpp/VWF-antigen ratio under steady state conditions, and changes in VWF clearance will therefore affect this ratio. We noticed that while VWF antigen levels increased, VWFpp levels remained unchanged, resulting in a decreased VWFpp/VWF-antigen ratio, which suggests that VWF clearance is delayed rather than that VWF production is increased. Second, clearance of VWF/KB-V13A12 is significantly slower in WT-mice compared to $FcRn^{KO}$-mice, not only underscoring the mechanism of delayed clearance but also demonstrating that this effect is FcRn-dependent.

When stored in Weibel-Palade bodies over a prolonged period of time, VWF is exposed to acidic conditions (pH=5.5), which is more acidic compared to the pH found in early/recycling endosomes (pH=6.2-6.5).[40,41] It seems unlikely therefore that passing through the mild acidic conditions in the early/recycling endosomes will change the functional and structural integrity of the VWF molecule. Indeed, no detectable changes in the VWF multimer pattern were detected when analyzing VWF multimers obtained from hVWD1-mice before and after treatment with KB-V13A12.[18] Data generated from both *in vitro* and *in vivo* assays further support the notion that VWF functionality remains intact.

In conclusion, we describe a novel bispecific nanobody that increases VWF antigen levels by delaying its clearance in an FcRn-dependent manner. The increased VWF levels obtained after a single subcutaneous injection are associated with an increased hemostatic potential, thereby correcting the bleeding tendency in hVWD1-mice. Preferably, one would like to raise VWF levels into the normal range (>50 IU/dl), as this will be associated with a near complete reduction in bleeding phenotype. Nevertheless, given the strong inverse correlation between bleeding score and VWF antigen/FVIII activity levels[42], any durable increase in VWF/FVIII levels could be beneficial in reducing the bleeding tendency in the patients.

KB-V13A12 could be considered as a potential candidate for a prophylactic treatment option for patients with VWD-type 1. Importantly, since the nanobody targets VWF in the circulation, it would be beneficial irrespective whether the reduced VWF levels originate from impaired biosynthesis/secretion or from increased clearance. Moreover, it seems plausible that the nanobody could be applicable for all VWD conditions where desmopressin treatment has been shown to be efficient either alone or in combination

with desmopressin). As such it could serve as a safer alternative treatment in cases where desmopressin treatment is contra-indicated (eg. because of cardiovascular comorbidities). Regarding the potential immunogenicity of the nanobody, both components of the bispecific nanobody share >90% sequence homology to the human IGHV3-23*04 germline gene, and have a humanness score of >95% after humanization. Furthermore, no anti-VHH antibodies could be detected in a repeated dosing experiment (Supplementary figure S3), which together suggest a low immunogenicity potential of the molecule.

Interestingly, several new drugs are being evaluated for their use in VWD, including VGA039 (an anti-protein S antibody), emicizumab (a bispecific antibody mimicking FVIII activity) and BT200 (an aptamer blocking both GpIbα and LRP-1 binding).[43,44] These molecules differ from KB-V13A12 in their mode of action. VGA039 and emicizumab correct the FVIII defect, whereas VWF defects remain unchallenged. BT200 increases VWF by blocking LRP1-mediated clearance, but since it interferes with the VWF/GpIbα interaction, it is less suitable for patients with reduced VWF activity.[45] Consequently, KB-V13A12 seems to be the most adapted molecule treat to VWD-type 1 patients, as it will increase both VWF and FVIII levels simultaneously. Extrapolating the half-life of the nanobody into the human context would suggest that one or two subcutaneous injections per month would result in a sustained increase of their endogenous VWF, providing a low-burden therapy allowing to improve both physical and mental quality of life. In addition, we believe that this approach could be extended to other pathologies associated with a quantitative deficiency of circulating plasma proteins.

Conflict of interest

IP, CC, ODC, PJL and CVD are inventors on a patent related to KB-V13A1. PJL receives research funding to the institute from BioMarin, Sanofi and E-therapeutics. CC receives research funding to the institute from Roche and NovoNordisk. Other authors declare no conflict of interest.

Author contributions

IP, CC, GM, EB, VL and CA performed experiments. IP, CC, SR, ODC, PJL and CVD analyzed data. IP, CC, CVD, PJL and OCD designed and supervised the study. PJL and CVD wrote the initial version of the manuscript and all authors contributed to its final editing.

Acknowledgements

This study received financial support from Agence Nationale de la Recherche (ANR-21-CE14-0076-01-VISTA) to CVD. We thank the Institut Biomédical du Val-de-Bièvre (IBVB-UMS44) for technical and facility support and the French Reference Center for von Willebrand disease (CRMW) for providing plasma samples.

References

1. Leebeek FW, Eikenboom JC. Von Willebrand's Disease. *N Engl J Med*. 2016;375(21):2067-2080.
2. Seidizadeh O, Eikenboom JCJ, Denis CV, et al. von Willebrand disease. *Nat Rev Dis Primers*. 2024;10(1):51.
3. Seidizadeh O, Cairo A, Baronciani L, Valenti L, Peyvandi F. Population-based prevalence and mutational landscape of von Willebrand disease using large-scale genetic databases. *NPJ Genom Med*. 2023;8(1):31.
4. Seidizadeh O, Cairo A, Oriani C, Peyvandi F. Global prevalence and ethnic diversity of von Willebrand disease: an updated population-based genetic analysis. *Research square*. 2025; doi.org/10.21203/rs.3.rs-6577209/vs1
5. Du P, Bergamasco A, Moride Y, Truong Berthoz F, Ozen G, Tzivelekis S. Von Willebrand Disease Epidemiology, Burden of Illness and Management: A Systematic Review. *J Blood Med*. 2023;14:189-208.
6. Srivaths L, Minard CG, O'Brien SH, et al. The spectrum and severity of bleeding in adolescents with low von Willebrand factor-associated heavy menstrual bleeding. *Blood Adv*. 2020;4(13):3209-3216.
7. Lavin M, Aguila S, Schneppenheim S, et al. Novel insights into the clinical phenotype and pathophysiology underlying low VWF levels. *Blood*. 2017;130(21):2344-2353.
8. Seidizadeh O, Ciavarella A, Baronciani L, et al. Clinical and Laboratory Presentation and Underlying Mechanism in Patients with Low VWF. *Thromb Haemost*. 2024;124(4):340-350.
9. Suvada K, Plantinga L, Vaughan CP, et al. Comorbidities, Age, and Polypharmacy Limit the Use by US Older Adults with Nocturia of the Only FDA-approved Drugs for the Symptom. *Clin Ther*. 2020;42(12):e259-e274.
10. Barr RD, Sek J, Horsman J, et al. Health status and health-related quality of life associated with von Willebrand disease. *Am J Hematol*. 2003;73(2):108-114.
11. de Wee EM, Mauser-Bunschoten EP, Van Der Bom JG, et al. Health-related quality of life among adult patients with moderate and severe von Willebrand disease. *J Thromb Haemost*. 2010;8(7):1492-1499.
12. Govorov I, Ekelund L, Chaireti R, et al. Heavy menstrual bleeding and health-associated quality of life in women with von Willebrand's disease. *Exp Ther Med*. 2016;11(5):1923-1929.
13. Xu Y, Deforest M, Grabell J, Hopman W, James P. Relative contributions of bleeding scores and iron status on health-related quality of life in von Willebrand disease: a cross-sectional study. *Haemophilia*. 2017;23(1):115-121.
14. Roberts JC, Kulkarni R, Kouides PA, et al. Depression and anxiety in persons with Von Willebrand disease. *Haemophilia*. 2023;29(2):545-554.
15. Sockolosky JT, Szoka FC. The neonatal Fc receptor, FcRn, as a target for drug delivery and therapy. *Adv Drug Deliv Rev*. 2015;91:109-124.
16. Qi T, Cao Y. In Translation: FcRn across the Therapeutic Spectrum. *Int J Mol Sci*. 2021;22(6).

17. Ober RJ, Martinez C, Lai X, Zhou J, Ward ES. Exocytosis of IgG as mediated by the receptor, FcRn: an analysis at the single-molecule level. *Proc Natl Acad Sci U S A*. 2004;101(30):11076-11081.
18. McCluskey G, Heestermans M, Peyron I, et al. A fully humanized von Willebrand disease type 1 mouse model as unique platform to investigate novel therapeutic options. *Haematologica*. 2024.
19. Denis C, Methia N, Frenette PS, et al. A mouse model of severe von Willebrand disease: defects in hemostasis and thrombosis. *Proc Natl Acad Sci U S A*. 1998;95(16):9524-9529.
20. Jumper J, Evans R, Pritzel A, et al. Highly accurate protein structure prediction with AlphaFold. *Nature*. 2021;596(7873):583-589.
21. Sugio S, Kashima A, Mochizuki S, Noda M, Kobayashi K. Crystal structure of human serum albumin at 2.5 A resolution. *Protein Eng*. 1999;12(6):439-446.
22. Fuller JR, Knockenhauer KE, Leksa NC, Peters RT, Batchelor JD. Molecular determinants of the factor VIII/von Willebrand factor complex revealed by BIVV001 cryo-electron microscopy. *Blood*. 2021;137(21):2970-2980.
23. Veyradier A, Boisseau P, Fressinaud E, et al. A Laboratory Phenotype/Genotype Correlation of 1167 French Patients From 670 Families With von Willebrand Disease: A New Epidemiologic Picture. *Medicine (Baltimore)*. 2016;95(11):e3038.
24. Buyue Y, Whinna HC, Sheehan JP. The heparin-binding exosite of factor IXa is a critical regulator of plasma thrombin generation and venous thrombosis. *Blood*. 2008;112(8):3234-3241.
25. McCluskey G, Heestermans M, Peyron I, et al. A fully humanized von Willebrand disease type 1 mouse model as unique platform to investigate novel therapeutic options. *Haematologica*. 2025;110(4):923-937.
26. Muczynski V, Casari C, Moreau F, et al. A factor VIII-nanobody fusion protein forming an ultrastable complex with VWF: effect on clearance and antibody formation. *Blood*. 2018;132(11):1193-1197.
27. Ayme G, Adam F, Legendre P, et al. A Novel Single-Domain Antibody Against von Willebrand Factor A1 Domain Resolves Leukocyte Recruitment and Vascular Leakage During Inflammation-Brief Report. *Arterioscler Thromb Vasc Biol*. 2017;37(9):1736-1740.
28. Lenting PJ, Westein E, Terraube V, et al. An experimental model to study the in vivo survival of von Willebrand factor. Basic aspects and application to the R1205H mutation. *J Biol Chem*. 2004;279(13):12102-12109.
29. Chaudhury C, Mehnaz S, Robinson JM, et al. The major histocompatibility complex-related Fc receptor for IgG (FcRn) binds albumin and prolongs its lifespan. *J Exp Med*. 2003;197(3):315-322.
30. Haberichter SL. von Willebrand factor propeptide: biology and clinical utility. *Blood*. 2015;126(15):1753-1761.
31. Haberichter SL. VWF propeptide in defining VWD subtypes. *Blood*. 2015;125(19):2882-2883.
32. Schulte S. Innovative coagulation factors: albumin fusion technology and recombinant single-chain factor VIII. *Thromb Res*. 2013;131 Suppl 2:S2-6.
33. Vanderschuren K, Arranz-Gibert P, Khang M, et al. Tuning protein half-life in mouse using sequence-defined biopolymers functionalized with lipids. *Proc Natl Acad Sci U S A*. 2022;119(4).

34. Yang B, Kim JC, Seong J, Tae G, Kwon I. Comparative studies of the serum half-life extension of a protein via site-specific conjugation to a species-matched or -mismatched albumin. *Biomater Sci*. 2018;6(8):2092-2100.
35. Swystun LL, Michels A, Lillicrap D. The contribution of the sinusoidal endothelial cell receptors CLEC4M, stabilin-2, and SCARA5 to VWF-FVIII clearance in thrombosis and hemostasis. *J Thromb Haemost*. 2023;21(8):2007-2019.
36. O'Sullivan JM, Ward S, Lavin M, O'Donnell JS. von Willebrand factor clearance - biological mechanisms and clinical significance. *Br J Haematol*. 2018;183(2):185-195.
37. Lenting PJ, Christophe OD, Denis CV. von Willebrand factor biosynthesis, secretion, and clearance: connecting the far ends. *Blood*. 2015;125(13):2019-2028.
38. Borvak J, Richardson J, Medesan C, et al. Functional expression of the MHC class I-related receptor, FcRn, in endothelial cells of mice. *Int Immunol*. 1998;10(9):1289-1298.
39. Akilesh S, Christianson GJ, Roopenian DC, Shaw AS. Neonatal FcR expression in bone marrow-derived cells functions to protect serum IgG from catabolism. *J Immunol*. 2007;179(7):4580-4588.
40. Terglane J, Menche D, Gerke V. Acidification of endothelial Weibel-Palade bodies is mediated by the vacuolar-type H+-ATPase. *PLoS One*. 2022;17(6):e0270299.
41. Yamashiro DJ, Maxfield FR. Regulation of endocytic processes by pH. *Trends Pharmacol Sci*. 1988;9(6):190-193.
42. Tosetto A, Rodeghiero F, Castaman G, et al. A quantitative analysis of bleeding symptoms in type 1 von Willebrand disease: results from a multicenter European study (MCMDM-1 VWD). *J Thromb Haemost*. 2006;4(4):766-773.
43. James P, Leebeek F, Casari C, Lillicrap D. Diagnosis and treatment of von Willebrand disease in 2024 and beyond. *Haemophilia*. 2024;30 Suppl 3:103-111.
44. Regling K, Sidonio RF, Jr. Factor VIII stimulants and other novel therapies for the treatment of von Willebrand disease: what's new on the horizon? *Expert Opin Pharmacother*. 2024;25(11):1427-1438.
45. Chion A, Byrne C, Atiq F, et al. The aptamer BT200 blocks interaction of K1405-K1408 in the VWF-A1 domain with macrophage LRP1. *Blood*. 2024;144(13):1445-1456.

Legends

Figure 1: Binding of KB-V13A12 to albumin and VWF

Panels A-B: Microtiter plates coated with recombinant human VWF (40 nM; *panel* A), human albumin (HSA; 100 nM; blue symbols; *panel* B) or mouse albumin (MSA; 100 nM; red symbols; *panel* B) were incubated with various concentrations of KB-V13A12 (0-33 nM and 0-667 nM, for *panels* A and B, respectively). Bound nanobody was probed using polyclonal peroxidase-labelled anti-cMyc antibodies. *Panel C:* Microtiter plates coated with HSA (blue symbols; 100 nM) or MSA (red symbols; 100 nM) were incubated with various concentrations of KB-V13A12 (0-50 nM) and a fixed concentration of recombinant VWF (24 nM). *Panel D:* Microtiter plates coated with HSA (blue & red circles; 100 nM) or MSA (pale blue & orange squares; 100 nM) were incubated with a fixed concentration of KB-V13A12 (0.2 μM) and various concentrations of recombinant VWF (0-36 nM). During incubations, pH was kept at pH=7.4 (blue & pale blue symbols) or pH-5.6 (red and orange symbols). Panels C-D: bound VWF was probed using polyclonal peroxidase-labelled anti-VWF antibodies. Data present mean±SD of three measurements.

Figure 2: Molecular modelling of KB-V13A12

Panel A: In silico simulation of KB-OptiAlb12 (coloured structures; 3D-model made using PDB-deposit 7CJ2 as template) docking on human albumin (PDB-deposit 1AO6). *Panel B: In silico* simulation of KB-VWF-013 (coloured structures; 3D-model made using PDB-deposit 4TVS as template) docking on human VWF-D'D3 region (PDB-deposit 6N29). For both panels, the top 30-ranked structures are shown. *Panel C:* Molecular for model of KB-V13A12 bridging albumin to the VWF-D'D3/FVIII complex. *Panel D:* Molecular for model of KB-V13A12 bridging albumin to the VWF-D'D3-A1/GpIbα complex. Figures were generated using PyMOL-software. *Panel E:* Human normal pooled plasma was spiked with KB-V13A12 (0-100 μg/ml) and VWF:GpIbR activity was measured. *Panel F:* Microtiter wells coated with VWF (1 μg/ml) were incubated with purified FVIII (0-3 U/ml) in the absence or presence of HSA (50 μg/ml), KB-V13A12 (50 μg/ml) or both at 50 μg/ml. Bound FVIII was probed using peroxidase-labelled polyclonal sheep anti-FVIII antibodies.

Figure 3: In vivo survival of KB-V13A12

Panel A: Biotinylated bivalent nanobody KB-VWF-006bv (2.5 mg/kg) was given intravenously to VWF-deficient mice (VWF-KO-mice; orange symbols) or wild-type mice (WT-mice; blue symbols), and KB-V13A12 (5 mg/kg; red symbols) was given intravenously to wild-type mice. Blood was collected at indicated time-points, and residual biotinylated nanobodies were measured. Presented is the relative residual nanobody (% of injected) versus time after

injection. *Panel B:* KB-V13A12 (5 mg/kg) was given subcutaneously to hVWD1-mice. Blood was collected at indicated time-points and residual KB-V13A12 levels were measured. Presented is the residual concentration of KB-V13A12 (in nM) versus time (days). *Panel C:* Concentrations of VWF (see Fig. 4) and KB-V13A12 were used to calculate the ratio KB-V13A12 for each of the time-points. Data represent mean±SD of 3-6 measurements/time-point.

Figure 4: KB-V13A12 increases VWF and FVIII levels

hVWD1-mice were given various doses of KB-V13A12 (0.5-25 mg/kg) subcutaneously. At indicated time-points blood was collected for the preparation of plasma in order to measure VWF antigen and FVIII activity levels. *Panel A:* Presented are VWF antigen levels (U/dl) at baseline (t=0) or after subcutaneous injection of KB-V13A12 *versus* time (days). *Panel B:* Presented are FVIII activity levels (U/dl) at baseline (t=0) or after subcutaneous injection of KB-V13A12 *versus* time (days). Four different doses were applied: 0.5 mg/kg (orange symbols), 2.0 mg/kg (red symbols), 5 mg/kg (blue symbols) and 25 mg/kg (green symbols). Data represent mean±SD of 3-12 measurements/time-point.

Figure 5: KB-V13A12 delays VWF clearance

Panel A: Four hVWD1-mice were each given KB-V13A12 (5 mg/kg). Before (T=0; red symbols) and 72h (blue symbols) after injection, blood samples were taken for the preparation of plasma to measure VWFpp and VWF antigen. Depicted is the ratio VWFpp over VWF antigen relative to T=0. Statistical analysis was performed using an unpaired Student's t-test. *Panel B:* C57B/6 mice were given human recombinant VWF (0.5 mg/kg), which was preincubated with KB-V13A12 or a control nanobody (both 5 mg/kg). At indicated time-points, blood samples were taken for the preparation of plasma to measure residual VWF levels. Presented are residual VWF concentration (% of injected) *versus* time (h). Data represent mean±SD of 3 experiments. *Panel C:* A similar experiment as described for panel B, except that proteins were injected into $FcRn^{KO}$-mice. *Panel D:* The area under the curve (AUC) values were calculated for each condition presented in *panels* B and C. Statistical analysis was performed using one-way ANOVA with Tukey's correction for multiple comparisons.

Figure 6: KB-V13A12 improves in vitro thrombus formation

Panels A-B: Heparin/PPACK-anticoagulated blood was obtained KB-V13A12-treated hVWD1-mice (5 mg/kg; given 3 days before blood collection). Blood from untreated hVWD1-mice, hVWD1-mice given histamine (13 μmol/kg; 30 min before blood collection) or hVWD1-mice given VWF (10 U/kg; 5 min before blood collection) were used as control. Blood was perfused over collagen in a parallel flow-chamber at 3000 s^{-1}. Percentage surface coverage is

represented in *panel* A, while representative images for each of the three conditions are shown in *panel* B. Data are mean±SD, with each symbol representing an individual experiment. Statistical analysis was performed using a one-way ANOVA test with Dunnett's correction for multiple comparisons.

Figure 7: KB-V13A12 improves the pro-haemostatic potential of hVWD1-mice
Panels A-B: Three days before injury, hVWD1-mice (n=11; red symbols) were given KB-V13A12 3 (5 mg/kg). 129S WT-mice (n=6; black symbols) and untreated hVWD1-mice (n=11; blue symbols) were used as control. Upon injury of the saphenous vein, clots formed were removed over a 30-min observation period, and the number of clots formed were noted. *Panel* A depicts the number of clots, with each symbol representing an individual mouse. *Panel* B shows the maximal bleeding time between clots. Statistical analysis was performed using a non-parametric Kruskal-Wallis test for multiple comparisons.

Figure 1
Bispecific nanobody KB-V13A12
Peyron *et al.*

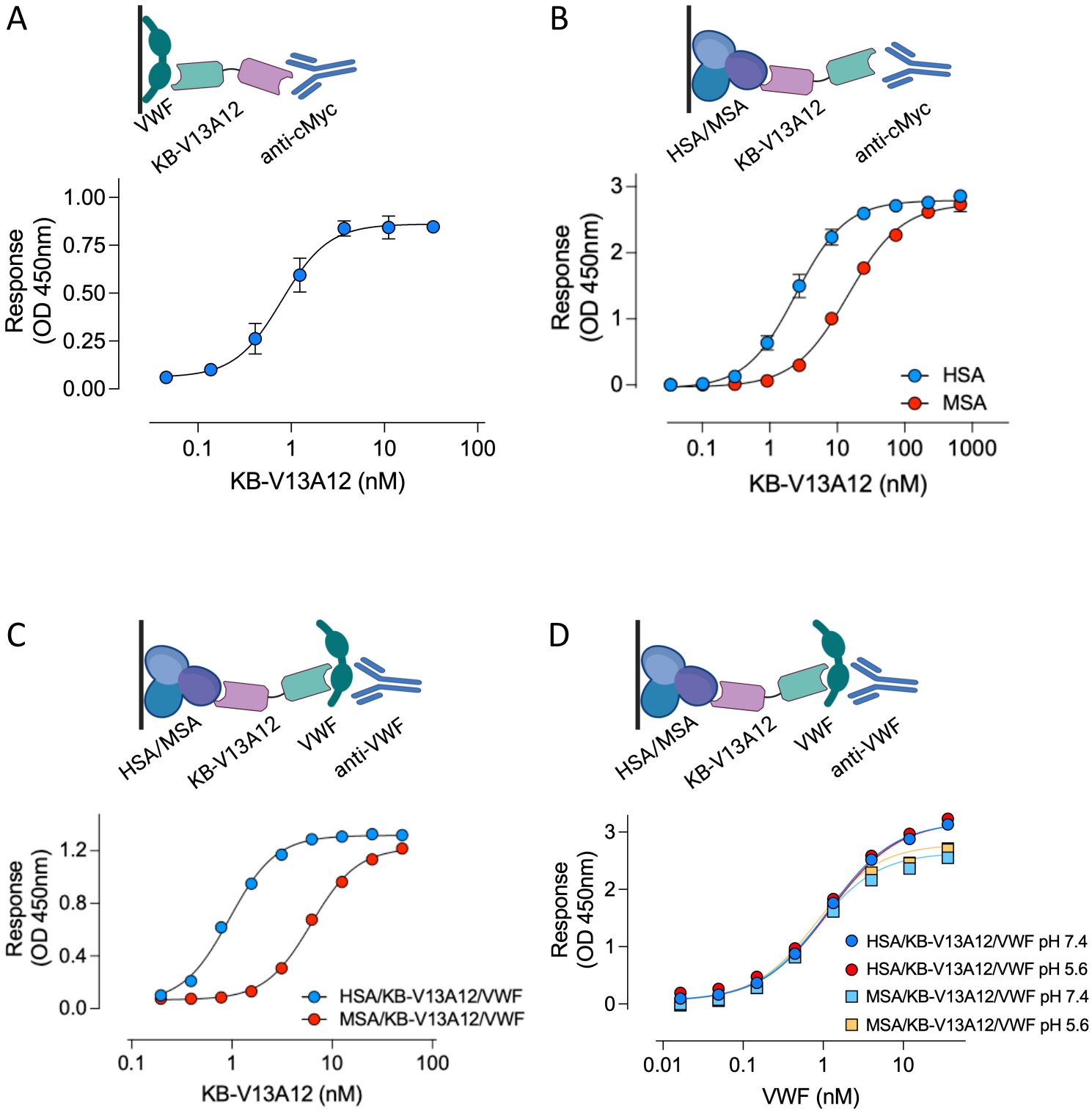

Figure 2
Bispecific nanobody KB-V13A12
Peyron *et al.*

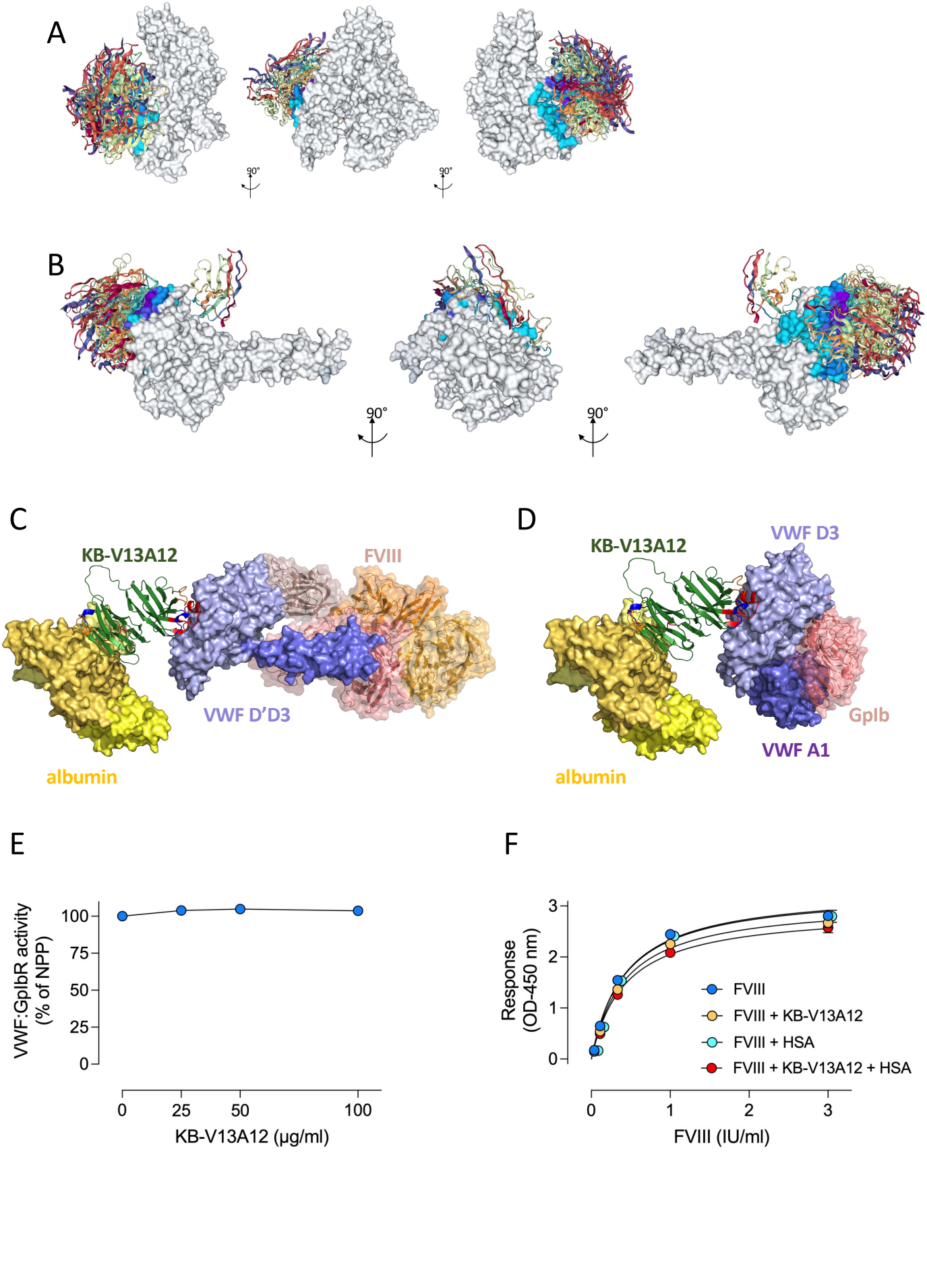

Figure 3
Bispecific nanobody KB-V13A12
Peyron *et al.*

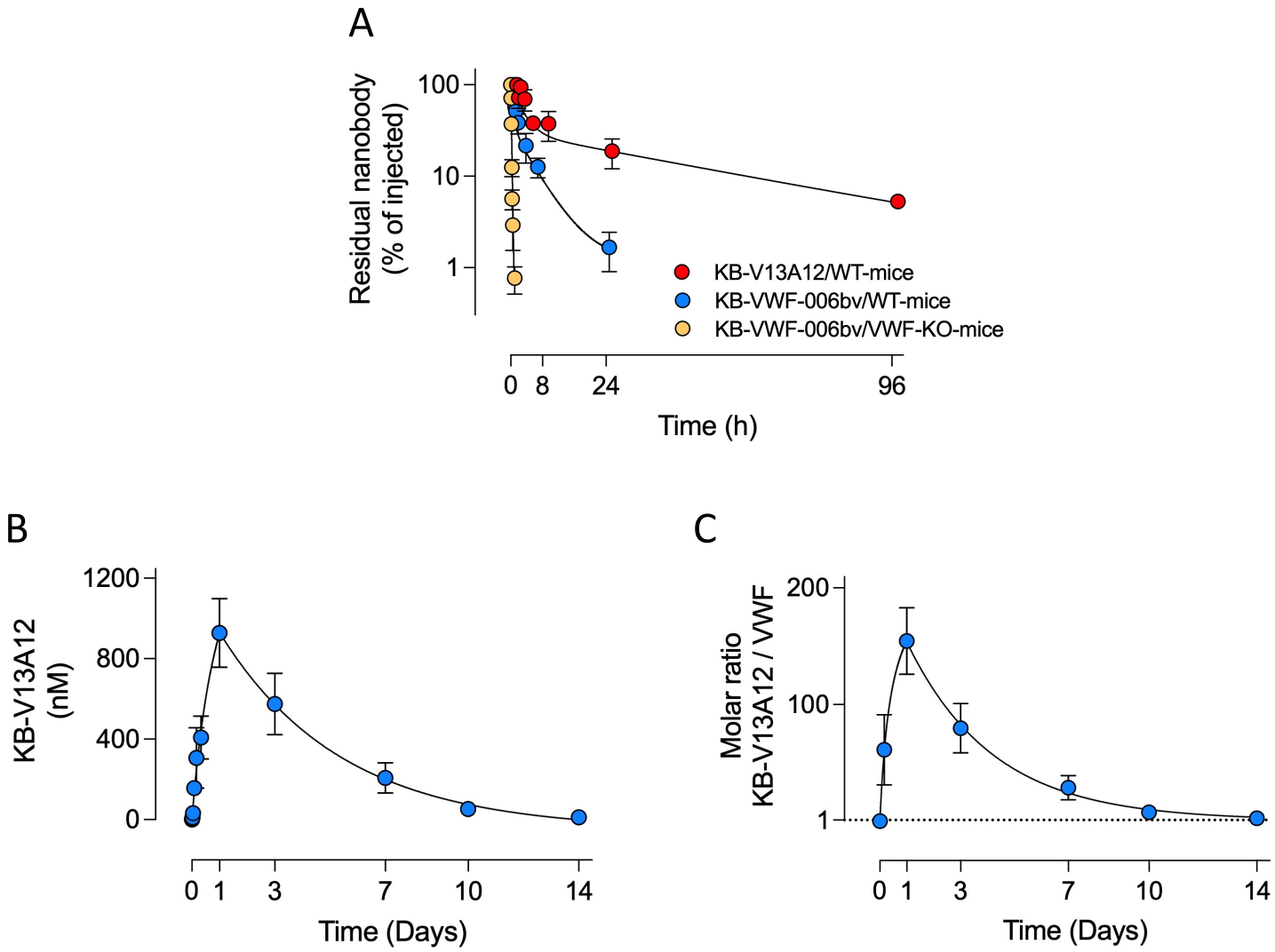

Figure 4
Bispecific nanobody KB-V13A12
Peyron *et al.*

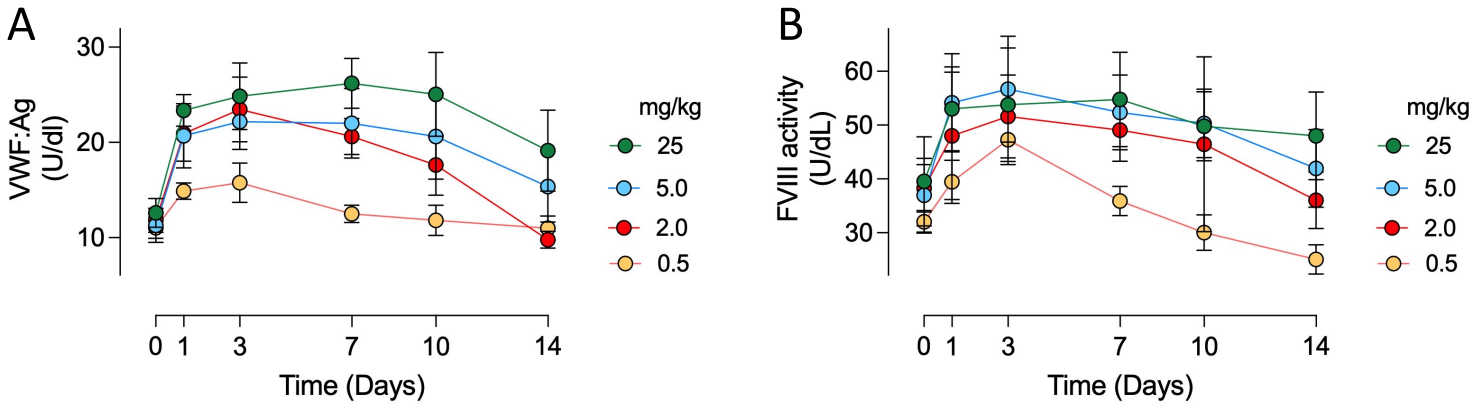

Figure 5
Bispecific nanobody KB-V13A12
Peyron *et al.*

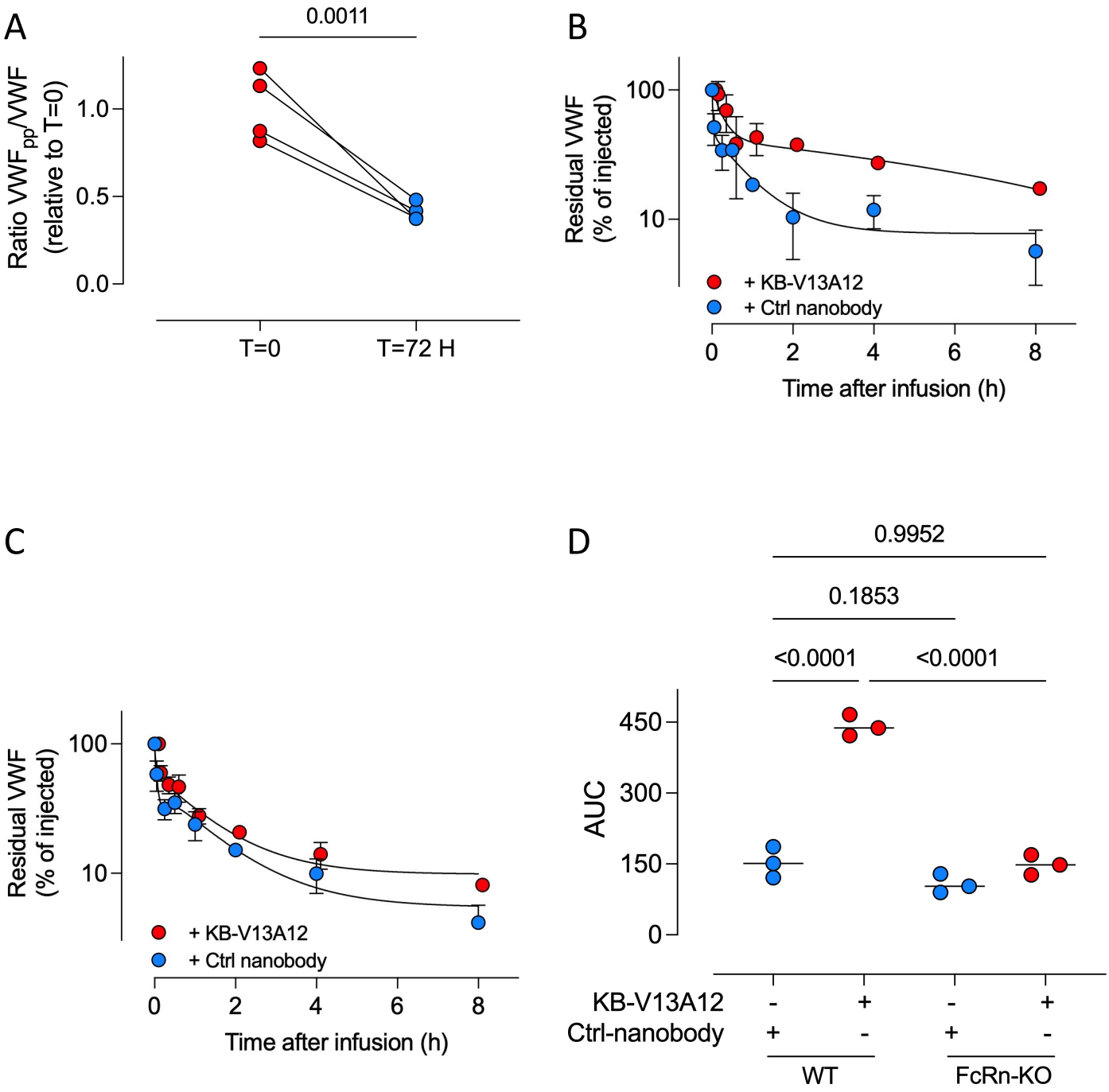

Figure 6
Bispecific nanobody KB-V13A12
Peyron *et al.*

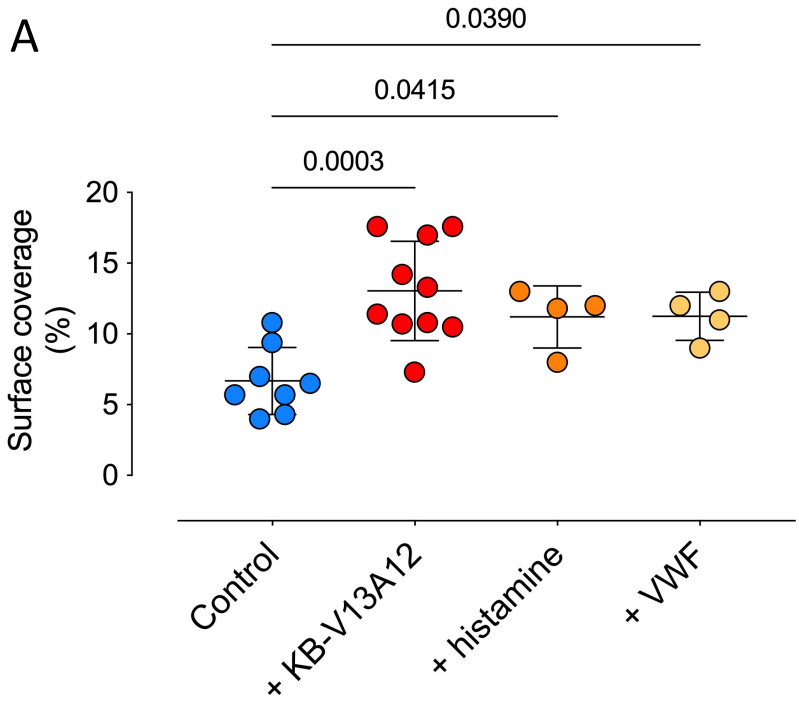

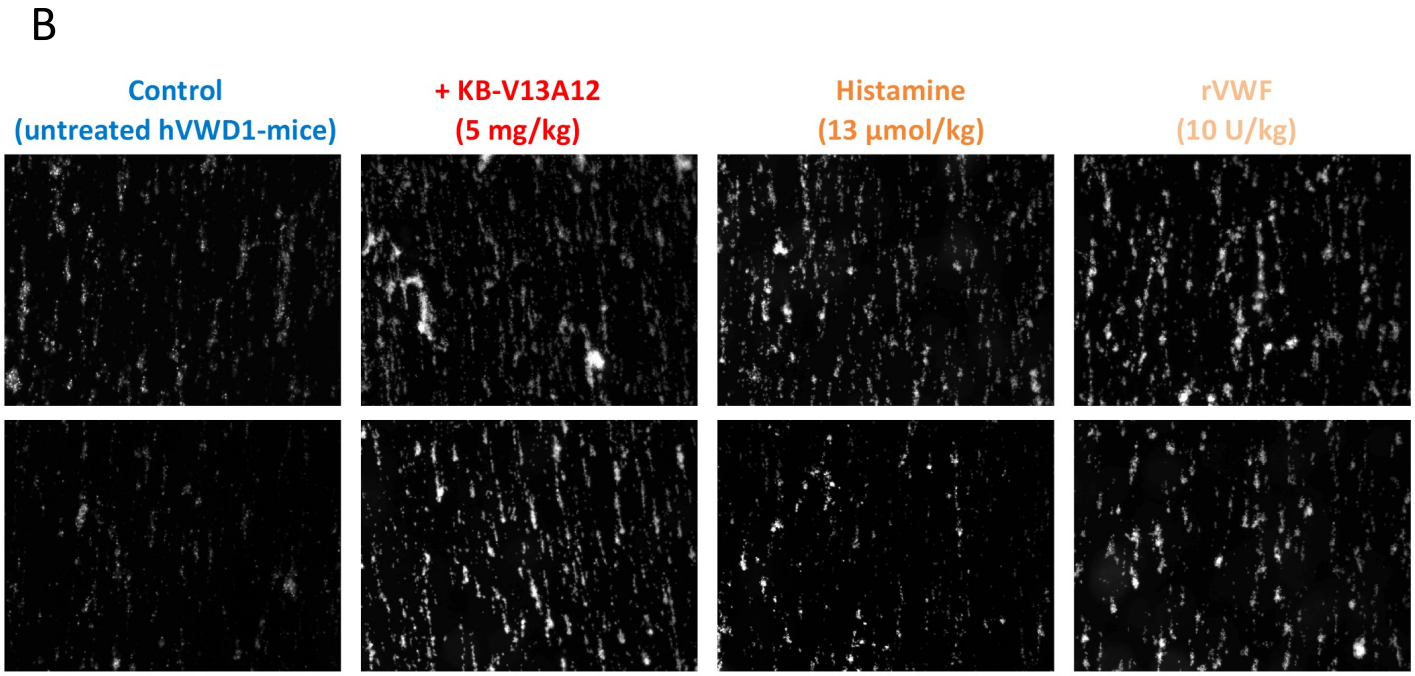

Figure 7
Bispecific nanobody KB-V13A12
Peyron *et al.*